

Discrete Time Crystal Order in Spin-Chains Enabled by Floquet Flat-Bands

Mahbub Rahaman^{1,*} and Anabha Roy^{2,†}

¹Harish Chandra Research Institute, A CI of Homi Bhabha National Institute,
Chhatnag Road, Jhansi, Prayagraj, Uttar Pradesh 211019, India

²Department of Physics, The University of Burdwan, Bardhaman, West Bengal 713104, India

We propose a novel protocol to realize discrete time-crystal (DTC) order in clean, periodically driven spin-1/2 chains. In each drive cycle, a global spin flip is followed by a two-tone flat-band segment. This flat-band segment engineers a fully degenerate Floquet quasienergy spectrum, suppresses thermalization, and stabilizes a robust period-doubled subharmonic response. Using exact time evolution, we identify a pronounced subharmonic peak at half the drive frequency in the Fourier spectrum of the order parameter, thereby providing clear evidence for the emergence of stable DTC. The resulting phase is insensitive to system size, interaction strength, and interaction range; however, it remains sensitive to spin-rotation errors (ε_r), which can destabilize the subharmonic response. Compared with disorder-induced many-body localized (MBL) and disorder-free dynamically many-body localized (DMBL) DTCs, we find that the exact flat-band protocol offers a broader tunability of drive parameters, whereas MBL and DMBL based DTCs are more resistant to ε_r . In particular, the ε_r sensitivity can be suppressed by incorporating additional spin-spin interactions that have modest deviations from the ideal flat-band protocol. This manifests itself in a robust DTC response over a finite window of spin-coupling strengths and drive frequencies. Our results establish flat-band driving as a versatile and experimentally relevant route to DTC order in disorder-free spin systems and motivate further exploration of non-equilibrium phases.

Keywords: Discrete time crystal, flat-band protocol, Out-of-equilibrium Floquet phases.

I. INTRODUCTION

Symmetry is a foundational principle in theoretical physics, underpinning quantum mechanics [1–6], quantum field theory [7–9], the Standard Model [10–12], condensed-matter physics [13, 14], and related areas [15]. Many infinite dimensional quantum systems exhibit spontaneous symmetry breaking (SSB), in which ground states do not inherit the full symmetry of the Hamiltonian [16]. A wide range of conventional phases of matter can be understood through SSB, making it central to phenomena such as magnetism and superfluidity [17, 18], quantum Hall effects [19, 20], and many-body localization that can protect or enable forms of symmetry breaking through athermality (eigenstate order) [21–24].

The SSB of translational symmetry is a core theme in equilibrium condensed-matter physics. For example, crystalline order arises from breaking the spatial translation symmetry. Analogously, in non-equilibrium dynamics, time-translation symmetry breaking (TTSB) refers to periodic dynamics that arises in the absence of explicit time-dependence [25, 26] or in periodically driven systems where the quasi-stationary state does not share the periodicity of the drive [27]. Wilczek’s original proposal of such Time Crystals—spontaneous periodic motion in classical [28] and quantum [29] equilibrium systems—was precluded by no-go theorems [30–32]. In the quest to obtain time crystals in closed quantum systems, this necessitated a change of focus to driven systems, where time periodicity enables Floquet or discrete time crystals (DTCs) [27, 33, 34] that were to be subsequently realized in trapped ions [35], superconducting qubits [36] and ultracold atoms [37].

In spin-1/2 chains, DTC order is associated with breaking

the global \mathbb{Z}_2 symmetry and is diagnosed through an order parameter \hat{O} evaluated in the state of out-of-equilibrium $|\psi(t)\rangle$. Defining $\mathcal{S}(t) \equiv \langle \psi(t) | \hat{O} | \psi(t) \rangle$, the hallmarks are: (a) TTSB, $\mathcal{S}(t) \neq \mathcal{S}(t+T)$ despite $\hat{H}(t) = \hat{H}(t+T)$; (b) rigidity, a robust subharmonic response with $\mathcal{S}(t) = \mathcal{S}(t+2T)$ without fine-tuning; and (c) persistence, stability of the dynamics of $2T$ over long times, including toward the thermodynamic limit.

The DTC order is operationally characterized by the presence of a robust subharmonic peak in the Fourier spectrum of the order parameter \hat{O} [38]. However, the eigenstate thermalization hypothesis (ETH) [39, 40] predicts that isolated quantum spin chains generically heat up and thermalize, leading to the eventual decay of the DTC order. Consequently, stabilization mechanisms are essential to maintain DTC phases. One prominent route is disorder-induced MBL [21, 22, 35], which suppresses heating by localizing many-body eigenstates and thus preserves memory of the initial state for long times. However, MBL stabilized DTC phases can remain vulnerable to internal excitations that trigger domain-wall proliferation and ultimately destroy the subharmonic response [41]. Alternative stabilization routes include integrable spin systems [42, 43], clean driven systems [44–49], and central-spin models [50, 51].

Although earlier theoretical and experimental realizations of DTC order predominantly relied on disorder-induced localization as a heating-suppression mechanism [34, 35, 52–55], an increasingly active direction has been the search for *clean* (disorder-free) routes to stabilizing subharmonic responses. In periodically driven spin models, such stabilization can arise from dynamical mechanisms that strongly slow down or suppress thermalization even in the absence of quenched randomness [44, 56, 57]. A widely explored paradigm is drive-induced *freezing*, in which the interplay of drive amplitude and frequency creates regimes where the stroboscopic evolution becomes nearly trivial for relevant initial states, thereby preventing rapid dephasing and thermalization [58–60]. This

* Primary & Corresponding author: mahbub.phys@gmail.com

† Co-Corresponding author: daneel@utexas.edu

phenomenon has been demonstrated across a range of clean systems, from effective two-level systems [61] to interacting spin chains, including nearest-neighbor transverse-field Ising models (TFIM) [58] as well as long-range spin-1/2 models [60]. In these cases, localization typically occurs only within structured regions of the drive-parameter space—often characterized by special values (“freezing points”) where the effective Floquet dynamics suppresses transitions and locks the system close to its initial configuration for long times. In long-range many-body systems (e.g., the Lipkin-Meshkov-Glick model), closely related effects can extend to disorder-free *dynamical many-body localization* (DMBL) [60], providing a qualitatively distinct mechanism for sustaining long-lived subharmonic order. These developments underscore the need for the suppression of thermalization in order to stabilize the DTC phases.

Furthermore, the transient nature of disorder-induced localization [22, 62] motivates the exploration of more versatile and tunable mechanisms to realize discrete time crystals. The flat-band protocol, recently explored in this context [63, 64], offers a promising alternative by engineering a completely degenerate quasi-energy spectrum through carefully articulated periodic drives. This engineered degeneracy localizes the system’s initial state, thereby suppressing thermalization. Notably, this mechanism remains effective across a wide range of interaction strengths and ranges, as well as diverse drive parameters, providing a flexible platform for realizing the DTC order in various spin models. The novelty of our work lies in adapting this two-toned flat-band drive protocol to a periodically driven spin-1/2 chain, where we demonstrate the emergence of a stable and resilient DTC phase.

We propose a protocol to realize a DTC phase in a clean, periodically driven spin-1/2 chain. Each driving cycle (with period $T = 2\pi/\omega$ and frequency ω) consists of a global spin-flip pulse followed by a flat-band segment. The latter is implemented via a two-tone drive that engineers a fully degenerate Floquet quasienergy spectrum, thus suppressing heating and stabilizing robust \mathbb{Z}_2 symmetry-breaking dynamics. Our exact time-evolution and Floquet numerical results demonstrate a stable $2T$ -subharmonic response, characterized by a pronounced peak at $\omega/2$ in the Fourier spectrum of magnetization. However, on longer timescales we observe a departure from the ideal flat-band behavior, where spin interactions begin to significantly influence the system’s dynamics. This interaction-driven evolution steers the system toward a thermal regime, giving rise to a prethermal discrete time crystal (DTC). We further quantify the robustness of the resulting phase against variations in spin-spin interaction strength and against spin-rotation errors. Compared with disorder-stabilized phases of MBL and DMBL induced DTCs, we found that flat-band-induced DTC is broadly independent of system size and interaction strengths or ranges, whereas MBL-based DTCs are comparatively more resilient to rotation errors. Finally, we show that incorporating an additional static interaction term within the flat-band segment can substantially enhance the robustness of the DTC order in the presence of spin-rotation errors within specific regions of drive frequency and spin-interaction parameter space. These results identify the flat-

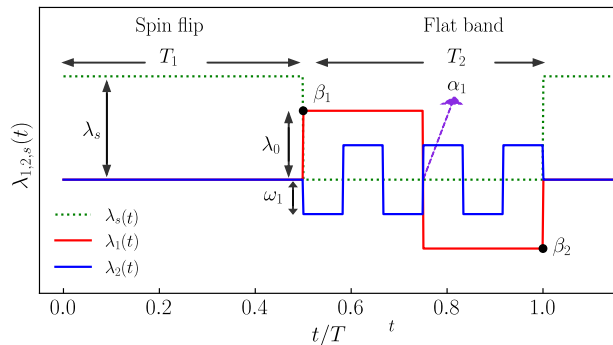


FIG. 1. Three time dependent drives $\lambda_{1,2,s}(t)$ protocol for the proposed flat-band DTC model. The first time interval, T_1 , consists of a spin-flip drive, while the second time interval, T_2 , consists of a flat-band protocol.

band driving protocol as a practical route to DTC order in disorder-free spin systems and motivate the experimental exploration of such non-equilibrium phases.

This article is organized as follows. Section II introduces the model and the driven dynamics, emphasizing the flat-band construction and its role in stabilizing the DTC order. Section III presents numerical evidence for the emerging DTC phase. Section IV analyzes stability with respect to variations in spin interaction strengths, ranges, and spin rotational errors. Section V compares the flat-band protocol with disorder-stabilized MBL and clean DMBL scenarios. Section VI explores the persistence of DTC against deviations from the ideal flat-band condition. Section VII concludes with a summary and outlook.

II. THE MODEL AND SYSTEM DYNAMICS

The generic flat-band protocol employs two-tone time dependent drives [65–67], specifically designed to ensure that the drive signals are out of phase whenever they switch polarities. This causes unit propagation at integer multiples of the time period, thus inducing a flat-band in the Floquet energy spectrum and consequently nullifying the dynamics of the system [63]. In principle, this protocol can be utilized to suppress heating and stabilize any subharmonic response to system and protocol defects. As a specific example, consider a one-dimensional spin-1/2 chain comprising N sites, driven by two time-dependent Hamiltonians $\hat{H}_{1,2}(t)$, expressed as:

$$\hat{H}(t) = \hat{H}_1(t) + \hat{H}_2(t) \quad (1a)$$

$$\begin{cases} \hat{H}_1(t) = \hat{H}_{\text{SF}}(t), & nT_1 < t \leq (n+1)T_1 \\ \hat{H}_1(t) = 0, & (n+1)T_1 < t \leq (n+2)T_1 \end{cases} \quad (1b)$$

$$\quad (1c)$$

$$\begin{cases} \hat{H}_2(t) = 0, & nT_2 < t \leq (n+1)T_2 \\ \hat{H}_2(t) = \hat{H}_{\text{FB}}(t), & (n+1)T_2 < t \leq (n+2)T_2 \end{cases} \quad (1d)$$

$$\quad (1e)$$

Here, \hbar is the reduced Planck's constant. In addition, $T_{1,2}$ are the time intervals between the n^{th} and $(n+1)^{\text{th}}$ turning points ($n = 0, 1, 2, \dots$) in the Hamiltonians $\hat{H}_{1,2}(t)$, respectively. By default, we set $T_1 = T_2 = T/2$, where T is the time-period of $\hat{H}(t)$. In Eq. (1b), the Hamiltonian is set to

$$\hat{H}_{\text{SF}}(t) = \lambda_s (1 - \varepsilon_r) \hbar \sum_{i=1}^N \hat{\sigma}_i^x. \quad (2)$$

Here, $\hat{\sigma}_i^{\mu=x,y,z}$ are the Pauli matrices at site i . Now, we consider the ideal case where $\varepsilon_r = 0$ ¹. If the value of λ_s is set to $\omega/2$ (where $\omega = 2\pi/T$, such that $\lambda_s T = \pi$; then the Hamiltonian \hat{H}_1 in Eq. (1b) simply flips each spin over the course of its duration. During this interval (T_1), the Hamiltonian $\hat{H}_1(t)$ does not incorporate any spin-spin interaction terms, thereby preserving the system's coherence. In the subsequent time interval, T_2 , the system's dynamics is governed by the flat-band protocol, represented by the Hamiltonian $\hat{H}_{\text{FB}}(t) = \sum_{l=1,2} \lambda_l(t) \hat{\Lambda}_l$, as illustrated in Fig. 1. The operators $\hat{\Lambda}_l$ are many-body in nature and satisfy the commutation relation $[\hat{\Lambda}_1, \hat{\Lambda}_2] \neq 0$. This protocol operates at dual rates, with the time-periodic functions $\lambda_l(t)$ having corresponding frequencies that are integer multiples of each other. The turning points at times $t_{1,2} = \beta_{1,2}T$, as depicted in Fig. 1 represent the instances where the Hamiltonian corresponding to Flat-band vanishes, i.e. $\hat{H}_{\text{FB}}(\alpha_1 T) = 0$, with $\alpha_1 = (\beta_1 + \beta_2)/2$.

A paradigmatic example of \hat{H}_{FB} is the transverse field Ising model (TFIM) with time-periodic fields, a prototypical example of an integrable spin chain². The periodic fields are utilized to construct the two-rate induced flat-band. The Hamiltonian for the TFIM-driven flat-band is expressed as:

$$\hat{H}_{\text{FB}}(t) = \lambda_1(t) J \hbar \sum_{i=1}^N \hat{\sigma}_i^x \hat{\sigma}_{i+1}^x + \lambda_2(t) h_z \hbar \sum_{i=1}^N \hat{\sigma}_i^z, \quad (3)$$

with periodic boundary conditions (PBC) $\sigma_{N+1}^\mu = \sigma_1^\mu$. Here, the time-dependent functions $\lambda_1(t)$ and $\lambda_2(t)$ are defined as

$$\begin{aligned} \lambda_1(t) &= +\lambda_0 & ; & \frac{mT}{4} < t \leq \frac{(m+1)T}{4}, \\ &= -\lambda_0 & ; & \frac{(m+1)T}{4} < t \leq \frac{(m+2)T}{4}, \\ \lambda_2(t) &= \omega_0 - \omega_1 & ; & \frac{qT}{4p} < t \leq \frac{(q+1)T}{4p}, \\ &= \omega_0 + \omega_1 & ; & \frac{(q+1)T}{4p} < t \leq \frac{(q+2)T}{4p}, \end{aligned} \quad (4)$$

where m, q are even natural numbers ($m, q = 0, 2, 4, \dots$), and $p \in \mathbb{Z}$. The quantity J represents the strength of the nearest-neighbor spin coupling, and h_z denotes the amplitude of the transverse field. For our numerical and analytical investigations, we have set the primary frequency ω of the time-dependent Hamiltonian $\hat{H}_{1,2}(t)$ to a default value of $\omega = 20$.

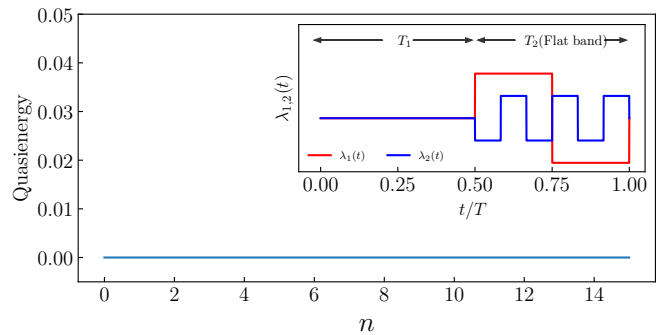


FIG. 2. Quasi-energy spectrum of the proposed flat-band protocol within the DTC model. Quasi-energy levels plotted against the quasi-energy eigenstates (n). The quasi-energy levels exhibit all-degeneracy at zero energy, indicating the emergence of the flat-band. The corresponding $\hat{H}_{\text{FB}}(T_2)$ drive protocol is illustrated in the inset.

Additional default values are $p = 3$, $\hbar = 1$, $\lambda_s = \omega/2 = 10$, $h_z = 1$, $\omega_0 = 0$, $\omega_1 = \lambda_0 J/2$, $J = 1$ and $\lambda_0 = 0.18$, as illustrated in Fig. 1. These settings ensure consistency with previous work [53], as well as minimal width of the Floquet spectrum [63]. Additionally, two time-dependent functions ($\lambda_{1,2}(t)$) with distinct amplitudes and frequencies are engineered to effectively nullify the dynamics of the system at the end of the drive-cycle, resulting in a pure degenerate flat-band (see Appendix-A).

To validate the emergence of this flat-band numerically, we have obtained and analyzed the quasi-energy spectrum. Specifically, we set $N = 8$ spins and simulated the time-evolution described in Eqs. (1). For this analysis, we disable the spin-flip drive, i.e., set $\hat{H}_1 = 0$ during the T_1 interval. This ensures that the dynamics is solely governed by the flat-band protocol $\hat{H}_{\text{FB}}(t)$ that is activated during the T_2 interval. The quasi-energy spectrum is obtained by diagonalizing the Floquet operator ($\hat{\mathcal{F}}$) at time T using the QuTiP module (Quantum Toolbox in Python [68]). According to Quantum Floquet theory [69–72], the time-evolution operator for a time-periodic Hamiltonian over one period T , given by $\hat{\mathcal{F}} = \mathcal{T} \exp \left[-i \int_0^T \hat{H}(t) dt / \hbar \right]$, where \mathcal{T} denotes time-ordering, produces eigenvalues that can be expressed as $e^{-i\varepsilon_\alpha T / \hbar}$, where ε_α are the quasi-energies defined modulo ω . The corresponding eigenstates, known as Floquet modes, satisfy $\hat{\mathcal{F}} |\phi_\alpha\rangle = e^{-i\varepsilon_\alpha T / \hbar} |\phi_\alpha\rangle$. The quasi-energy spectrum provides information on the long-time dynamics of periodically driven systems.

The quasi-energy spectrum exhibits complete degeneracy, with all levels collapsing to zero energy, as illustrated in Fig. 2. This confirms that the flat-band protocol effectively localizes the spin-chain wavefunction and can suppress thermalization. Upon activating \hat{H}_1 and repeatedly applying the complete drive protocol described in Eqs. (1), the spins are expected to return to their initial configuration at even multiples of the time period, thereby exhibiting period-doubling behavior. This periodic recurrence violates the intrinsic discrete time-translation symmetry of the driven system, giving rise to a DTC phase with $2T$ periodicity. The following section presents a detailed

¹ Small values of ε_r have been introduced during the stability analysis described in Sect. IV

² We also consider non-integrable long-range models in Sect. IV

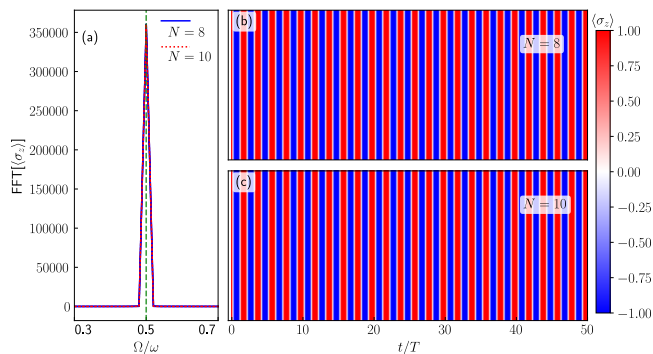


FIG. 3. Temporal evolution of the magnetization $\langle \hat{\sigma}^z(t) \rangle$ for the proposed DTC model in spin chains of sizes $N = 8$ and $N = 10$, with the spin rotational error fixed at $\varepsilon_r = 0$. The magnetization oscillates within the range $[-1, 1]$ at each discrete time period, demonstrating a clear $2T$ periodicity, as depicted in panels (b) and (c). The left panel (a) illustrates the FFT of the magnetization, highlighting a distinct subharmonic peak at $\omega/2$ for both system sizes, thereby confirming the realization of the DTC phase.

numerical investigation of this emergent DTC phase.

III. EMERGENCE OF THE DTC

We numerically simulated the complete drive protocol described in Eqs. (1) for long times, with \hat{H}_{FB} set to Eq. (3). Specifically, we ran two instances comprising $N = 8$ and $N = 10$ spins, respectively. In both instances, the spin chain was initially prepared in a fully spin-polarized state. Additionally, we turn off the spin rotation error ($\varepsilon_r = 0$), while keeping all other parameters consistent with Sect. II. Simulations were performed to evaluate the propagator in QuTiP, and the results were utilized to compute the time evolution of the order parameter which, in this case, is the magnetization $\langle \hat{\sigma}^z(t) \rangle = \langle \psi(t) | \hat{\sigma}^z | \psi(t) \rangle$. As shown in Fig. 3(b-c), the magnetization displays a clear $2T$ -periodicity, although the underlying primary drive is T -periodic. This corroborates the breaking of discrete time-translation symmetry and confirms the emergence of a DTC phase in the spin chain. To further corroborate the emergence of the DTC phase, we compute the Fourier spectrum of the magnetization $\langle \hat{\sigma}^z(t) \rangle$ over an extended time window, as illustrated in Fig. 3(a). The spectrum exhibits a pronounced subharmonic peak at $\Omega = \omega/2$, without any other discernible features, thus unambiguously confirming the $2T$ -periodic nature of the dynamics. The absence of additional spectral peaks, together with the non-extensive behavior of both the magnetization and its Fourier transform, can be attributed to the complete quasi-energy degeneracy engineered by the flat-band protocol. This engineered degeneracy not only ensures the temporal resilience of the DTC phase, but also underpins its persistence over a larger system size ($N = 10$), underscoring the scalability of the proposed mechanism.

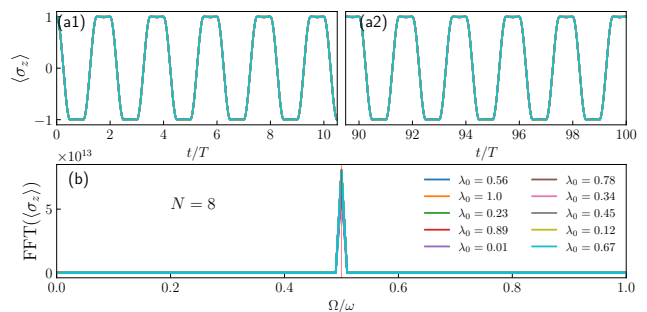


FIG. 4. The top panel (a) illustrates the temporal variation of the magnetization $\langle \hat{\sigma}^z(t) \rangle$ for the proposed DTC model in a spin chain of size $N = 8$, subjected to varying spin-spin interaction strengths. The bottom panel (b) presents the FFT of the corresponding magnetization, revealing the presence of a subharmonic peak at $\omega/2$ for all values of λ_0 .

IV. STABILITY AND RIGIDITY OF THE FB-DTC

In the preceding sections, we demonstrated the emergence of the DTC phase stabilized with Floquet flat-bands, provided that the spins and the underlying system are prepared under ideal conditions. These conditions include the absence of spin rotational errors (*i.e.*, $\varepsilon_r = 0$), a DTC drive that is tuned to perform the spin-flip operations, a perfectly two-toned exact flat-band protocol, and the exclusive presence of nearest-neighbor spin-spin interactions with coupling strength ($\lambda_0 J = 0.18$) as specified in Eq. (3). To evaluate the robustness of the proposed model under more realistic scenarios, we now simulate deviations from these ideal conditions and investigate the stability of the DTC phase.

We begin by investigating the stability of the DTC phase with respect to variations in the *spin-spin interaction strength* that range from very small to relatively large values. Numerical simulations are performed for different values of $\lambda_0 J \in [0.01, 1]$, while keeping all other parameters consistent with those outlined in Sect. II, specifically $\omega = 20$, $\varepsilon_r = 0$, $h_z = 1$, $\omega_0 = 0$, $\omega_1 = \lambda_0 J/2$, and $\lambda_s = \omega/2 = 10$. The temporal evolution of magnetization is computed and presented in Fig. 4(a1-a2). The results reveal that the $2T$ -DTC phase emerges robustly across the entire range of spin-spin interaction strengths and remains stable over extended timescales. This highlights the resilience of the DTC phase to variations in spin-spin interaction strength and underscores the effectiveness of the flat-band protocol in suppressing ETH [39, 40, 60, 63].

Furthermore, we have investigated the stability of the DTC phase across various *spin-spin interaction ranges*, characterized by the power-law decay form $J_{ij} = J/|i-j|^\beta$ for the $(i, j)^{\text{th}}$ spin-pair. Here, the flat-band Hamiltonian is modified from the paradigmatic example in Eq. (3) to

$$\hat{H}_{\text{FB}}(t) \rightarrow \lambda_1(t) \hbar \sum_{i < j} J_{ij} \hat{\sigma}_i^x \hat{\sigma}_j^x + \lambda_2(t) h_z \hbar \sum_i \hat{\sigma}_i^z, \quad (5)$$

Here, β denotes the interaction-range parameter. Following Buyskikh's benchmarking [73], we consider physically distinct regimes of β : $\beta = 0$ (all-to-all interactions), $\beta = 1.5$

and $\beta = 2.5$ (long-range interactions), and $\beta = \infty$ (inf), corresponding to nearest-neighbor interactions, i.e., the paradigmatic case in Eq. (3). We performed numerical simulations for spin-chain sizes $N = 8, 10$ and computed the parity-adjusted order parameter $Z(nT) \equiv (-1)^n \langle \psi(nT) | \hat{\sigma}^z | \psi(nT) \rangle$ over long timescales (up to $10^6 T$) in these interaction regimes. The results, shown in Fig. 5, indicate that the DTC phase emerges across all interaction ranges and remains robust for long durations in both system sizes. However, at later times, the order parameter exhibits a gradual decay in the all-to-all case ($\beta = 0$), with a slightly faster decay rate than in the shorter-range cases ($\beta = 1.5, 2.5, \infty$). This trend suggests comparatively stronger thermalization effects in the all-to-all regime, although overall decay remains weak and the DTC response persists on extended timescales for all β . At asymptotically long times, the system exhibits a gradual drift toward thermal equilibrium. This behavior reflects the deviation from the flat-band, arising from spin-spin interactions, and is consistent with the presence of a prethermal discrete time crystal (DTC) phase within the proposed model.

To further assess the stability of the DTC phase, we introduce a small finite *spin rotational error* ($\varepsilon_r > 0$) into the Hamiltonian \hat{H}_1 , as defined in Eq. (1b). Numerical simulations are performed for $\varepsilon_r \in \{0.01, 0.03, 0.05, 0.1, 0.15, 0.2\}$ with the spin chain size fixed at $N = 8$, while all remaining parameters are maintained at the values specified in Sect. II. The temporal evolution of magnetization, presented in Fig. 6(a–f), reveals the emergence of characteristic beat patterns for each nonzero rotational error, signifying the presence of spectral components beyond the subharmonic frequency $\Omega = \omega/2$. To identify these additional frequencies, we performed an FFT of the magnetization time data; the resulting spectra are shown in Fig. 6(g). The FFT reveals distinct sidebands in the vicinity of $\Omega = \omega/2$, which are responsible for the observed beating in the magnetization dynamics. As shown in the inset of Fig. 6(g), the beat frequency $\delta\Omega_B$ increases with ε_r , reflecting a progressive destabilization of the DTC phase. Collectively, these results underscore the sensitivity of the flat-band-induced DTC phase to spin-rotational imperfections, highlighting the importance of precise pulse-angle control for maintaining a stable subharmonic response.

V. COMPARATIVE ROBUSTNESS OF DTC PHASES: FLAT-BAND VS MBL/DMBL

We have investigated the robustness of the flat-band (FB)-induced DTC order in relation to two widely studied localization mechanisms: disorder-induced MBL and drive-induced DMBL in a clean system. Using numerical simulations, we assess the stability of DTC through time-resolved magnetization and Fourier analysis, with particular focus on the beat frequency $\delta\Omega_B$ corresponding to the subharmonic peak. The following subsections present the comparative results and highlight the parameter regimes in which each mechanism remains the most resilient to spin-rotation errors and variations in interaction range.

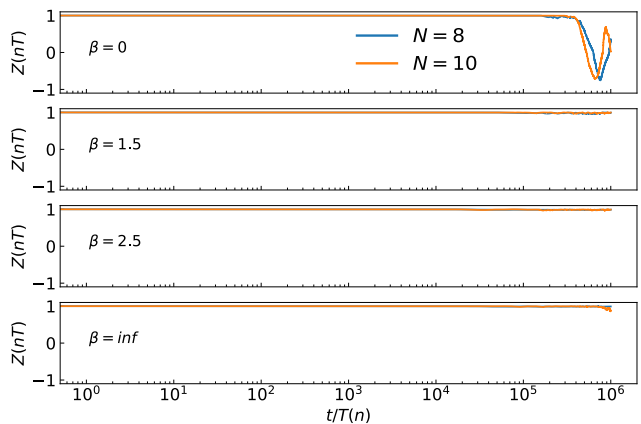


FIG. 5. Temporal evolution of the magnetization order parameter, $Z(nT) = (-1)^n \langle \hat{\sigma}^z(nT) \rangle$, at stroboscopic times for system sizes $N = 8, 10$ and various spin-spin interaction ranges ($\beta = 0, 1.5, 2.5, \infty$ (inf)).

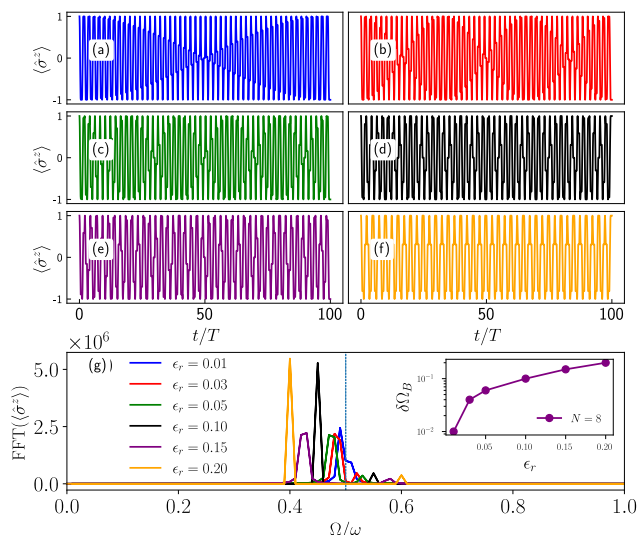


FIG. 6. Panels (a–f) display the temporal evolution of the magnetization $\langle \hat{\sigma}^z(t) \rangle$ for a spin chain of $N = 8$ sites under systematically increasing spin-rotation errors ($\varepsilon_r = 0.01, 0.03, 0.05, 0.1, 0.15, 0.2$). With growing ε_r , the initially perfect period-doubled oscillations gradually develop beating patterns, indicating the appearance of spectral components beyond the primary subharmonic frequency $\Omega = \omega/2$. Panel (g) shows the corresponding FFT spectra, where well-resolved sidebands emerge in the vicinity of $\Omega = \omega/2$ (marked by a dotted blue vertical line). As illustrated in the inset, the beat frequency $\delta\Omega_B$ increases with ε_r , offering a quantitative signature of the progressive melting of the DTC phase induced by finite spin-rotational imperfections.

A. Stability comparison of FB-DTC with disorder MBL-DTC

We have investigated the robustness of the DTC phase induced by the flat-band protocol in comparison to that of the DTC phase stabilized via MBL. To that end, we follow the

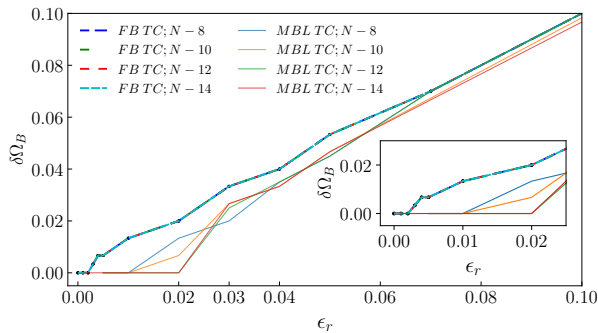


FIG. 7. Comparison of the beat frequency of the magnetization $\langle \hat{\sigma}^z(t) \rangle$ for the FB-DTC (dashed curves) and the MBL-DTC phase (solid curves, averaged over 960 disorder realizations) across different spin chain sizes $N = 8, 10, 12, 14$. The magnetization is evaluated over a duration of $300T$. The beat frequency ($\delta\Omega_B$) is plotted as a function of the spin rotational error (ϵ_r). The inset provides a magnified view of the main plot for enhanced clarity.

seminal work of Yao et al. [53], which provides a comprehensive investigation into the emergence and stability of the MBL stabilized DTC phase in a one dimensional spin-1/2 chain. The Hamiltonian governing the MBL induced DTC is given by Eqs. (1) with the flat-band Hamiltonian modified from the paradigmatic example in Eq. (3) to the following.

$$\hat{H}_{\text{FB}} \rightarrow \hat{H}_{\text{MBL}} = \sum_{i=1}^N J' \hat{\sigma}_i^z \hat{\sigma}_{i+1}^z + \sum_{i=1}^N B_i^z \hat{\sigma}_i^z. \quad (6)$$

Here, the random field B_i^z is sampled from a uniform distribution within the range $[0, W]$, where $W = 2\pi$ represents the strength of the disorder, consistent with previous studies [53]. Additionally, the spin coupling strength is fixed at $J' = 0.18$ to ensure the localization of the system and the stability of the DTC phase, as indicated by its level spacing ratio ($\langle r \rangle \approx 0.38$) [52, 53]. Next, we investigate the dynamics governed by the drive protocols outlined in Eqs. (1 and 6), with disorder strength B_i^z uniformly distributed in the range $[0, 2\pi]$. Simulations are conducted for spin chain sizes $N = 8, 10, 12, 14$, with the DTC drive parameters set to default values. To assess the impact of spin rotational errors, we introduce a set of errors, ϵ_r , into the Hamiltonian $\hat{H}_{\text{SF}}(t)$, as defined in Eqs. (1b) and 2. The temporal evolution of magnetization $\langle \hat{\sigma}^z(t) \rangle$ is numerically computed from $t = 0$ to $300T$, and averaged over 960 disorder realizations. Additionally, we performed an FFT of the magnetization data to identify the dominant frequencies and quantify the associated beat frequencies ($\delta\Omega_B$). For comparison, we also present results from an analysis of the aforementioned quantities for the DTC induced by the flat-band protocol as described in Eqs. (1-1e) for the same set of rotational errors.

The results of this comparative analysis are presented in Fig. 7, revealing significant differences in the variation of $\delta\Omega_B$ between the FB-DTC and the MBL-DTC. The FB-DTC phase appears to be resilient to spin rotation errors up to $\epsilon_r \approx 0.002$, beyond which $\delta\Omega_B$ increases linearly with ϵ_r . In contrast, the MBL-DTC phase demonstrates resilience up to $\epsilon_r \approx 0.01$, followed by a regime (up to $\epsilon_r \sim 0.02$) where $\delta\Omega_B$ decreases with

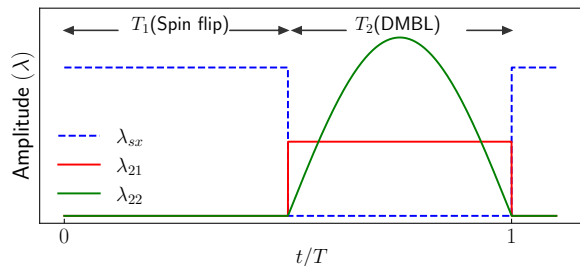


FIG. 8. Schematic representation of the drive protocol for the proposed dynamical localization-induced DTC model in a clean spin-1/2 system. The protocol consists of two time-dependent drives: a spin-flip drive (λ_{sx}) applied during the first time interval T_1 , followed by a time-dependent transverse field Ising model (TFIM) or Lipkin-Meshkov-Glick (LMG) model (λ_{21}) driven by a sinusoidal field with amplitude λ_{22} during the second time interval T_2 .

increasing spin chain length. For larger ϵ_r , the beat frequency begins to increase linearly, approaching the scaling observed for the FB-DTC phase. These findings indicate that the FB stabilized DTC phase is more susceptible to spin rotational errors than the MBL stabilized DTC phase. The inset of Fig. 7 provides a magnified view of the main plot for improved clarity. Thus, the MBL-DTC phase exhibits superior robustness against spin rotational errors relative to the FB-DTC phase.

B. Stability Comparison of FB-DTC with DMBL-DTC

We now extend our investigation beyond the basic comparison with MBL-DTC to comparative studies of the stabilization of the flat-band DTC phase with DTC-phases obtained in clean systems where emergent localization mechanisms arise intrinsically from the dynamics via Dynamical Many Body Localization. In the context of spin chains, dynamical localization can give rise to localized states that resist thermalization, thereby providing a robust mechanism for stabilizing DTC phases.

To that end, we consider a spin-1/2 chain governed by the DMBL induced DTC protocol detailed in Eqs. (1) with the flat-band Hamiltonian modified from the paradigmatic example in Eq. (3) to the following.

$$\hat{H}_{\text{FB}} \rightarrow \hat{H}_{\text{DMBL}}(t) = \sum_{i<j} J_{ij} \hat{\sigma}_i^y \hat{\sigma}_j^y + \lambda_{22}(t) \sum_{i=1}^N \hat{\sigma}_i^z, \quad (7)$$

with power-law decay over the range β in the spatial interaction amplitudes $J_{ij} = J_0/|i-j|^\beta$, and spin coupling J_0 . The physically distinct ranges of β -are classified according to Buyskikh's benchmarking detailed in Sect. IV. The transverse field drive $\lambda_{22}(t) \equiv h \sin(\omega t)$ is characterized by a time-dependent amplitude modulated by the drive frequency ω and the amplitude h , as illustrated in Fig. 8. Consequently, the time-dependent Hamiltonian $\hat{H}_2(t)$ implemented during the second time interval T_2 comprises the TFIM for $\beta = \infty$ and the LMG model for $\beta = 0$ [60]. Note that the drive protocol during the T_1 -cycle remains unchanged from the default protocol described

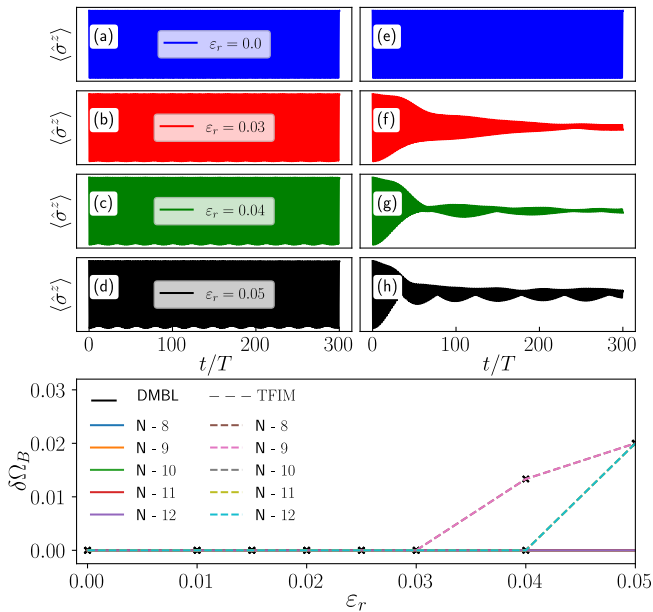


FIG. 9. Temporal evolution of magnetization for different spin rotational errors $\varepsilon_r = (0.0, 0.03, 0.04, 0.05)$ for DMBL (columns a, b, c, d) and TFIM (columns e, f, g, h) localized DTCs over long timescales up to $300T$ for a spin chain of size $N = 9$. The DMBL-induced DTC phase remains robust against ε_r , whereas the TFIM-induced DTC phase exhibits faster melting as ε_r increases. The bottom panel (i) shows the beat frequencies ($\delta\Omega_B$) around $\Omega = \omega/2$ for different ε_r values, calculated from the magnetization data for various spin chain lengths ($N = 8, 9, 10, 11, 12$). While no $\delta\Omega_B$ is observed for the DMBL-induced DTC phase (solid lines), finite $\delta\Omega_B$ emerges for the TFIM-induced DTC phase (dashed lines) when $\varepsilon_r \geq 0.03$.

in Eqs. 1b and 2, thereby preserving the recurrence of spin-flips and maintaining TTSB. Crucially, when the drive parameters h and ω are tuned such that the ratio $\kappa \equiv 4\omega/h$, coincides with a root of the zeroth-order Bessel function of the first kind, such that $\mathcal{J}_0(\kappa) = 0$, the system becomes dynamically localized in its initial state throughout the second time interval T_2 [44, 58, 60]. This condition, commonly referred to as the *freezing point*, is characteristic of the high-frequency drive regime. In the low-frequency regime, on the contrary, no such localization occurs, and the system fails to retain memory of its initial state.

We investigate the stability of the DTC phase facilitated by dynamical localization in a spin chain of size $N = 9$, considering both the TFIM ($\beta = \infty$) and the LMG model ($\beta = 0$). The spin chain is initialized in a fully polarized up-spin configuration. The drive parameters are set to $\omega = 20$ and $J_0 = 0.18$, with the drive amplitude (h) tuned to correspond to the freezing points of the system. Additionally, spin rotational errors ($\varepsilon_r = 0.0, 0.01, 0.02, 0.03, 0.04, 0.05$) are introduced during spin-flip operation in the first time interval T_1 . The spin-flip drive is applied for a duration of $T_1 = T/2$, followed by the TFIM or LMG Hamiltonian during the remaining interval $T_2 = T/2$. Numerical simulations are conducted to compute the temporal evolution of magnetization $\langle \hat{\sigma}^z(t) \rangle = \langle \psi(t) | \hat{\sigma}^z | \psi(t) \rangle$. As can easily be seen in

Fig. 9, magnetization exhibits $2T$ -periodicity despite the primary drive being T -periodic, thus confirming the emergence of a DTC phase in the spin chains. There are visible differences between the TFIM- and DMBL-induced DTC cases in the disintegration of the subharmonic due to finite spin rotation errors. The DMBL-DTC phase is extremely robust against finite spin rotational errors, whereas the subharmonic exhibits greater sensitivity for the TFIM-DTC case. This difference highlights the role of non-integrability in localization: the integrable TFIM model is more susceptible to perturbations, while the non-integrable LMG model maintains localization more robustly. The beat frequencies around $\Omega = \omega/2$ are obtained from the FFT decompositions for sizes ($N = 8, 9, 10, 11, 12$) (see Fig. 9). For the TFIM-induced DTC phase, beats appear for finite $\varepsilon_r \geq 0.03$ in systems with $N \geq 9$. In contrast, the DMBL-induced DTC phase does not exhibit any beats around $\Omega = \omega/2$ even for comparatively larger rotation errors (up to $\varepsilon_r = 0.05$). However, in comparison to the FB-DTC phase, the DMBL- and TFIM-DTC phases demonstrate greater resilience to finite spin rotational errors. As shown in Fig. 7, the beat frequency of the flat-band-induced DTC phase begins to rise even for relatively small $\varepsilon_r \gtrsim 0.002$, while the DMBL- and TFIM-DTC phases remain stable under similar conditions. This indicates that the flat-band-induced DTC phase is more sensitive to finite spin rotational errors compared to the DMBL- and TFIM-induced DTC phases.

VI. PERSISTENT DTC UNDER IMPERFECT FLAT-BANDS

The flat-band protocol introduced in Sect. II is designed to achieve perfect localization: the two-tone drive is carefully tuned so that the effective Floquet operator reduces to the identity at integer multiples of the time period, thereby freezing all dynamics (see Appendix A). In practice, however, precise realization of such a protocol is challenging, and small deviations from the ideal drive parameters are inevitable. Rather than merely degrading performance, such imperfections can, in certain cases, even confer additional stability to the system. To explore both effects, we examine two types of departure from the ideal flat-band: (i) small perturbations in the frequencies of the two time-dependent flat-band drives, and (ii) the inclusion of an additional spin-spin interaction term in the faster-rotating component of the two-tone drive.

A. Deviation in the frequencies in the perfect flat-band

To model the above imperfections, we consider modified flat-band drive parameters expressed as:

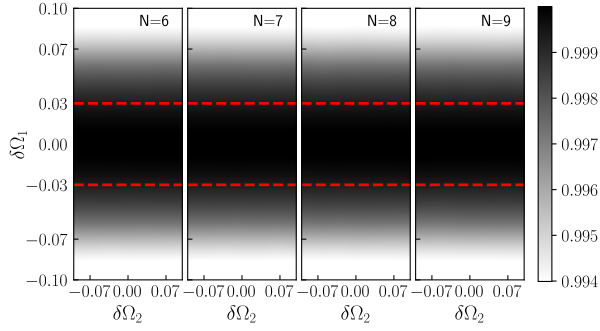


FIG. 10. Fidelity of the DTC phase as a function of deviations $\delta\Omega_1$ and $\delta\Omega_2$ for system sizes $N = 6, 7, 8, 9$. The fidelity remains high within the range of small deviations (bounded by the red lines), demonstrating the robustness of the DTC phase against imperfections in the drive frequencies.

$$\begin{aligned}
 \lambda_1(t) &= +\lambda_0 && ; \frac{mT'}{4} < t \leq \frac{(m+1)T'}{4}, \\
 &= -\lambda_0 && ; \frac{(m+1)T'}{4} < t \leq \frac{(m+2)T'}{4}, \\
 \lambda_2(t) &= -\omega_1 && ; \frac{qT''}{4p} < t \leq \frac{(q+1)T''}{4p}, \\
 &= +\omega_1 && ; \frac{(q+1)T''}{4p} < t \leq \frac{(q+2)T''}{4p}, \quad (8)
 \end{aligned}$$

Here, $\delta\Omega_1$ and $\delta\Omega_2$ represent small deviations in the drive frequencies such that $T' = 2\pi/(\omega + \delta\Omega_1)$ and $T'' = 2\pi/(p\omega + \delta\Omega_2)$. All other parameters are kept consistent with the default values specified in Sect. II. To quantify the impact of these imperfections, we calculate the fidelity of the system's state, defined as $F(2nT)$, where:

$$F(t) = |\langle \psi(0) | \psi(t) \rangle|^2 \quad (9)$$

Here, $|\psi(0)\rangle$ denotes the initial state, and $|\psi(t)\rangle$ represents the state of the system at stroboscopic times corresponding to integer multiples of the double period, $t = 2nT$ (with $n = 1, 2, 3, \dots$) [44]. A high fidelity value ($F(t) \equiv 1$) indicates that the system remains close to its initial state, serving as a key metric to evaluate the robustness of the DTC phase.

To systematically assess the impact of these imperfections, we numerically compute the fidelity for spin chains of sizes $N = 6, 7, 8, 9$ over a duration of $100T$, sweeping the deviations $\delta\Omega_1$ and $\delta\Omega_2$ across a range of values. As shown in Fig. 10, the fidelity remains close to unity when the deviations are small ($\delta\Omega_1, \delta\Omega_2 \in [-0.03, 0.03]$), confirming that the DTC phase tolerates minor imperfections in the drive frequencies without appreciable degradation. However, as the deviations grow in magnitude, the fidelity gradually decreases, signaling a progressive loss of stability in the DTC phase. These observations paint a nuanced picture: while the flat-band protocol possesses an intrinsic resilience to practical imperfections, maintaining optimal performance still demands careful control over the drive parameters. In other words, the protocol is forgiving up to a point, but not unconditionally.

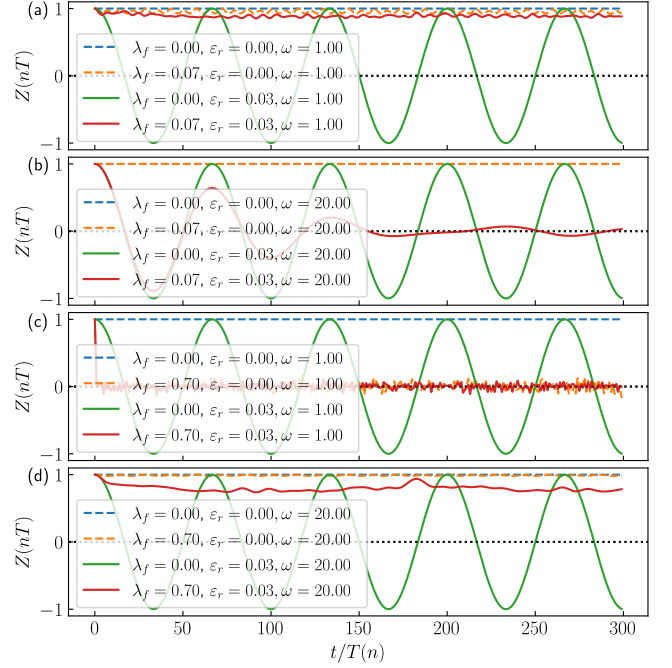


FIG. 11. Temporal evolution of the magnetization order parameter $Z(nT)$ under the modified flat-band protocol incorporating an additional spin-spin interaction term, evaluated for various values of $\lambda_{0,f}$, ω_0 , ϵ_r , and drive frequency ω . The results demonstrate that the DTC phase exhibits resilience to spin-rotation errors ($\epsilon_r = 0.03$) in regimes characterized by strong interactions and high-frequency ($\omega = 20$) driving (panel-d), as well as in regimes with weak interactions and low-frequency ($\omega = 1$) driving (panel-a).

B. Introduction of additional spin-interaction term

To further investigate the robustness of the flat-band-induced DTC in the presence of spin-rotational errors under imperfect flat-band conditions, we introduce an *additional aperiodic spin-spin interaction* along the order parameter direction (z-direction) into the two-tone flat-band Hamiltonian and examine its influence on the emergent localization properties of the spin chain. Specifically, we consider a modified time-periodic flat-band Hamiltonian of the form:

$$\tilde{H}_{\text{FB}}(t) = \lambda_1(t) \sum_i \hat{\sigma}_i^x \hat{\sigma}_{i+1}^x + \lambda_2(t) \sum_i \hat{\sigma}_i^z + \lambda_f J \sum_i \hat{\sigma}_i^z \hat{\sigma}_{i+1}^z, \quad (10)$$

where the time-dependent coefficients are defined the same as in Eq. (4). Additionally, λ_f represents the additional term for the spin-spin interaction strength and time coefficients are fixed at $m, q = 0, 2, 4, \dots$ and $p = 3$ for numerical simulations. To analyze the dynamics, we decompose the time evolution operator over one period into five intervals and apply the Magnus expansion:

$$\hat{U}(T, 0) = \exp(-i\hat{H}_{\text{ME}}T), \quad (11)$$

where \hat{H}_{ME} is the effective Hamiltonian expanded as a series in powers of the drive frequency. The effective Hamiltonian

(see Appendix B for detailed derivations) is given by:

$$\hat{H}_{\text{ME}} \equiv \frac{\lambda_f J}{2} \sum_i \hat{\sigma}_i^z \hat{\sigma}_{i+1}^z + \frac{\lambda_s(1 - \varepsilon_r)}{2} \sum_i \hat{\sigma}_i^x + \hat{O}(T). \quad (12)$$

The first term represents the additional spin-spin interaction, the second term corresponds to the spin-flip operation, and the third term accounts for the leading-order correction arising from their interplay.

To analyze the DTC dynamics under this modified flat-band protocol, we investigate the exact DTC-Hamiltonian in different regimes of drive frequency and interaction strength. For strong interactions ($\lambda_0 J \sim 1$) and high-frequency driving ($\omega \sim 20$), the correction term becomes negligible, allowing the effective Hamiltonian to be dominated by the additional spin interaction and spin-flip terms. This ensures robust localization and a stable subharmonic response, even in the presence of spin-rotation errors. In contrast, in the low-frequency regime ($\omega \sim 1$), the last term becomes significant, introducing complex dynamics that can destabilize the DTC phase. However, for weaker interactions ($\lambda_0 J \sim 0.1$), the spin-spin interaction term becomes negligible under high-frequency driving, making the system more susceptible to spin-rotation errors. However, in the low frequency regime, the last term remains small due to the smaller amplitudes despite the low frequency. The additional spin interaction term effectively becomes large due to the small frequency and counteracts the additional spin rotational error, eventually obtaining robust DTC.

We investigate this argument numerically by simulating the time evolution of the magnetization order parameter $Z(nT) \equiv (-1)^n \langle \hat{\sigma}_i^z(nT) \rangle$ under the modified flat-band protocol for various values of $\lambda_f J = 0.7\lambda_0 J$, $J = 1$, $\omega_0 = 0$ for $\lambda_0 \in \{1, 0.1\}$, and $\omega \in \{1, 20\}$, in the presence of spin-rotation error ($\varepsilon_r = 0.03$) for a spin chain of size $N = 8$. The results, depicted in Fig. 11, reveal that the DTC phase remains robust against spin-rotation errors in regimes characterized by strong interactions and high-frequency driving, as well as in regimes with weak interactions and low-frequency driving. Therefore, the flat-band protocol with an additional spin-spin interaction term can stabilize the DTC phase under specific regimes of drive frequency and interaction strength.

VII. SUMMARY AND OUTLOOK

In this work, we have introduced a novel framework for realizing DTC phases in clean spin-1/2 chains by combining a global spin-flip operation with a flat-band drive protocol. The flat-band protocol is meticulously designed to produce a fully degenerate quasi-energy spectrum, thereby localizing the system's initial state and suppressing thermalization. This is achieved through the application of two distinct periodic drives, ensuring that the time evolution operator reduces to the identity at each discrete time period. The resulting dynamics stabilizes the periodic flipping of spins, leading to robust period-doubling behavior that breaks intrinsic time-translation symmetry, thereby enabling the emergence of a DTC phase.

Our analysis reveals that the flat-band-induced DTC phase exhibits remarkable stability across a wide range of spin-

spin interaction strengths and interaction ranges. However, it demonstrates sensitivity to spin rotational errors, which manifest as rapid oscillations and beat patterns in the dynamics. However, the DTC phase persists for small deviations of the drive parameters from the ideal flat-band condition, as evidenced by high fidelity values. At stroboscopic times, the time evolution operator reduces to the identity, a hallmark of the flat-band protocol. Although this property primarily implies that the flat-band protocol does not induce dynamics, over sufficiently long times, we find that a crossover to a thermal regime can occur due to spin-spin interactions with various interaction ranges. This leads to the emergence of a prethermal DTC phase, enabled by the flat-band protocol, which is distinct from trivial period-doubling phases.

We further conducted a comparative study of the stability of the flat-band-induced DTC phase against those stabilized by disorder-induced MBL and disorder-free DMBL. The results indicate that the flat-band-induced DTC phase is more susceptible to spin rotational errors than the MBL- and DMBL-induced DTC phases. Among these, the DMBL-induced DTC phase demonstrates superior robustness to spin rotational errors relative to the transverse field Ising model (TFIM)-induced DTC phase. Additionally, the flat-band-induced DTC phase exhibits resilience to variations in interaction strengths and ranges, unlike the MBL- and TFIM-induced DTC phases, which are significantly influenced by these parameters [53, 54, 56, 74]. Notably, the flat-band-induced DTC phase remains independent of system size, offering a distinct advantage over the MBL- and DMBL-induced DTC phases, particularly in the thermodynamic limit.

To further enhance the robustness of the DTC phase against spin rotational errors, we explored a modified flat-band protocol that incorporates an additional spin-spin interaction term. This modification significantly improves the stability of the DTC phase, particularly in regimes characterized by strong interactions and high-frequency driving, as well as in regimes with weak interactions and low-frequency driving. These findings suggest that the flat-band protocol can be engineered to mitigate the effects of spin-rotation errors, thereby enhancing the robustness of the DTC phase under realistic conditions.

Outlook: The proposed flat-band-induced DTC framework paves the way for exploring non-equilibrium phases in clean spin systems. Its reliance on engineered drive sequences, rather than disorder, makes it particularly suitable for implementation on Noisy Intermediate-Scale quantum devices (NISQ) [75]. Experimental platforms such as trapped ions [35], superconducting qubits [36], and Rydberg atom arrays [76] are well-suited to implement this protocol. For instance, in trapped ions, the global spin-flip operation and flat-band drive can be realized using laser-induced spin-dependent forces and tailored pulse sequences. In superconducting qubits, microwave control fields can generate the required time-dependent Hamiltonians, while Rydberg atom arrays can utilize optical tweezers and Rydberg blockade mechanisms to engineer the desired interactions. However, achieving effective suppression of the system dynamics requires a deeper understanding of the mechanisms governing the stability of the DTC phase, including the potential role of disorder in mitigating the

faster oscillating components of the flat-band protocol [63].

Although the exact flat-band-induced DTCs phase does not achieve the same level of robustness as the MBL-induced DTC phase in the presence of spin rotational errors [53], it offers a versatile and experimentally accessible route to realization of DTCs in clean driven systems. In contrast to DMBL-induced time crystals, which require fine-tuning of the drive parameters to achieve localization and subharmonic response [60], the flat-band protocol provides a wider parameter space for stabilizing the DTC phases. This flexibility makes it particularly advantageous for experimental platforms where disorder is challenging to implement or control.

In conclusion, the flat-band protocol significantly broadens the scope of time crystal realization, offering a robust and scalable approach to achieving DTC phases in clean, disorder-free systems. Future research could explore the interplay between drive engineering, interaction range, and error resilience, potentially uncovering new regimes of non-equilibrium quantum order.

ACKNOWLEDGMENTS

MR thanks DST, India, for support through the DST/FFT/NQM/QSM/2024/3 project. AR acknowledges support from the University Grants Commission (UGC) of India, Grant No. F.30-425/2018(BSR), as well as from the Science and Engineering Research Board (SERB), Grant No. CRG/2018/004002. Both authors express their sincere appreciation to Dr. Sayan Choudhury of the Harish-Chandra Research Institute for insightful discussions and valuable feedback on the manuscript.

AUTHOR CONTRIBUTIONS

MR: Conceptualization, Data curation, Project administration, Formal analysis, Investigation, Methodology, Resources, Software, Visualization, Writing – original draft; **AR:** Resources, Conceptualization, Writing – review & editing;

Appendix A: Emergence of Flat band

Using Eq. (4), the symmetry inherent in the periodic drive dictates that

$$\lambda_{1,2}(\alpha_1 T + t') = -\lambda_{1,2}(\alpha_1 T - t'), \quad (\text{A1})$$

for $t' \leq (\beta_2 T - \beta_1 T)/2$. This ensures that for all t' ,

$$\hat{H}_{\text{FB}}(\alpha_1 T + t') = -\hat{H}_{\text{FB}}(\alpha_1 T - t'). \quad (\text{A2})$$

The time evolution operator $\hat{U}(t)$, governed by the Schrödinger equation $i\hbar\partial_t\hat{U}(t) = \hat{H}(t)\hat{U}(t)$, can be expressed as

$$\begin{aligned} \hat{U}(T, 0) &= \mathcal{T} \exp\left(-i \int_0^T \hat{H}(t'') dt''\right), \\ &= \mathcal{T} \exp\left(-i \int_{T_1}^T \hat{H}_{\text{FB}}(t'') dt''\right) \exp\left(-i \int_0^{T_1} \hat{H}_1(t'') dt''\right), \end{aligned} \quad (\text{A3})$$

where \mathcal{T} denotes the time-ordering operator. Given the high drive frequencies, we can apply the first-order Suzuki-Trotter decomposition (STD) [77] to approximate the time evolution operator as

$$\begin{aligned} \hat{U}(T, 0) &\approx \prod_{m=0}^N \left\{ \exp(-i\hat{H}_{\text{FB}}(t_m)\Delta t) + O(\Delta t^2) \right\} \\ &\quad \cdot \exp\left(-i\lambda_s(1 - \varepsilon_r) \sum_i \hat{\sigma}_i^x\right), \end{aligned} \quad (\text{A4})$$

where $\Delta t = (T - T_1)/(1 + N)$. Given the high effective frequency of the flat-band drive (2ω), we can utilize the Zassenhaus' formula [44, 78–80] for two operators \hat{a} and \hat{b} , which can be expressed as:

$$e^{\hat{a}+\hat{b}} = e^{\hat{a}} e^{\hat{b}} \prod_{n=2}^{\infty} e^{P_n(\hat{a}, \hat{b})}, \quad (\text{A5})$$

where $P_n(\hat{a}, \hat{b})$ represents the polynomial n -th of \hat{a} and \hat{b} . Consequently,

$$e^{T_1(\hat{a}+\hat{b})} = e^{T_1\hat{a}} e^{T_1\hat{b}} e^{P_2 T_1^2[\hat{a}, \hat{b}]} e^{P_3 T_1^3[\hat{a}, [\hat{a}, \hat{b}]]} \dots \approx e^{T_1\hat{a}} e^{T_1\hat{b}}, \quad (\text{A6})$$

where higher-order terms $O(T_1^2)$ can be neglected. Applying the Zassenhaus formula in Eq.(A6) to the time evolution operator, we obtain

$$\hat{U}(T, T_1) \equiv \prod_{m=0}^N \exp[-i\hat{H}_{\text{FB}}(t_m)\Delta t]. \quad (\text{A7})$$

With proper time ordering, the time evolution operator can be written as

$$\hat{U}(T, T_1) = \prod_m \hat{U}(t_{m+1}, t_m) = \prod_m \hat{U}_m. \quad (\text{A8})$$

The evolution operator $\hat{U}(T, T_1)$ operates between the turning points β_1 and β_2 . The null point $\hat{H}(\alpha_1 T) = 0$ implies that $\hat{U}(\alpha_1 T_2 + \Delta t, \alpha_1 T_2) = \mathbf{1}$. By applying the STD along with the Zassenhaus' formula, we can approximate the time evolution operator $\hat{U}(T, T_1)$ as follows:

$$\begin{aligned} \hat{U}(T, T_1) \equiv & \hat{U}(\beta_2 T_2, \beta_2 T_2 - \Delta t) \hat{U}(\beta_2 T_2 - \Delta t, \beta_2 T_2 - 2\Delta t) \dots \\ & \dots \hat{U}(\alpha_1 T_2 + 2\Delta t, \alpha_1 T_2 + \Delta t) \hat{U}(\alpha_1 T_2, \alpha_1 T_2 - \Delta t) \dots \hat{U}(\beta_1 T_2 + 2\Delta t, \beta_1 T_2 + \Delta t) \hat{U}(\beta_1 T_2 + \Delta t, \beta_1 T_2). \end{aligned} \quad (\text{A9})$$

It should be noted that the extreme terms in Eq. (A9) are exact Hermitian conjugates of each other, as indicated by Eq. (A2). This results in:

$$\hat{U}(T, T_1) = \mathbf{1}. \quad (\text{A10})$$

Therefore, the unitary evolution operator becomes:

$$\hat{U}(T, 0) = \exp(-i\hat{H}_{SF}T_1). \quad (\text{A11})$$

Furthermore, the Hamiltonian $\hat{H}(t)$ is time periodic, and therefore does not conserve energy. Using *Floquet theory*, one can explain the dynamics of the system in terms of k 'th quasi-stationary eigenstates ($\Phi^k(n)$) and the corresponding quasi-stationary eigenvalues ($\Phi^k(E)$), thereby transforming the time dependent problem to time independent problem. The system propagator is derived from the Schrödinger equation, $i\hbar\partial_t\hat{U}(t) = \hat{H}(t)\hat{U}(t)$. The time evolution of the system is governed by the Floquet Hamiltonian, which is a time-independent operator constructed from the time-dependent Hamiltonian of the system. The floquet operator is defined as

$$\hat{\mathcal{F}} = \exp(-i\hat{H}_F T), \quad (\text{A12})$$

here, \hat{H}_F is the Floquet Hamiltonian and T is the drive time period. The Floquet Hamiltonian is derived from the time-dependent Hamiltonian of the system $\hat{H}(t)$, as, $\hat{H}_F = \left(\hat{H}(t) - i\frac{\partial}{\partial t}\right)$, evaluated in the stroboscopic time interval $t = nT$; $n = 1, 2, 3, \dots$.

Taking the Floquet operator as $\hat{\mathcal{F}}$, the effective Floquet Hamiltonian (\hat{H}^{eff}) for the proposed model in T time is given by

$$\begin{aligned} \hat{\mathcal{F}} &= \exp(-i\hat{H}^{\text{eff}}T) \\ &= \exp(-i\hat{H}_2 T_2) \exp(-i\hat{H}_1 T_1) \end{aligned} \quad (\text{A13})$$

To understand the system's dynamics during the second time interval, governed solely by the flat-band protocol, we can disregard the spin-flip operation ($\hat{H}_1(t)$) in Eq. (1). This simplifies Eq. (A3) to:

$$\hat{U}(T, 0)_{\text{FB}} \equiv \mathcal{T} \exp\left(-i \int_{T_1}^T \hat{H}_{\text{FB}}(t'') dt''\right) = \mathbf{1}. \quad (\text{A14})$$

Thus, the reduced Floquet operator in the absence of the spin-flip drive is given by:

$$\hat{\mathcal{F}} = \exp(-i\hat{H}^{\text{eff}}T) = \exp(-i\hat{H}_{\text{FB}}T_2), \quad (\text{A15})$$

$$\text{and, } \hat{\mathcal{F}} = \hat{U}(T, 0)_{\text{FB}} = \mathbf{1}. \quad (\text{A16})$$

These equations, Eqs. (A15)-(A16), imply that $\hat{H}^{\text{eff}} = 0$, leading to quasi-energy $\Phi^k(E) = 0$ for all n 'th Floquet states, thereby manifesting a completely degenerate *flat* band.

Appendix B: Flat-band Protocol: In presence of additional Interaction

The exact flat-band protocol outlined in Sect. II yields perfectly unitary dynamics, independent of system size and interaction strength. As demonstrated in Sect. VI, this protocol exhibits robustness against small perturbations in the two-tone drive frequencies. However, the introduction of considerable spin-rotation errors during the T_1 interval can induce rapid oscillations and beat patterns in the system's dynamics, potentially undermining localization and the subharmonic response. This sensitivity arises from the intrinsic mechanism of the flat-band protocol, which achieves dynamical suppression by engineering a fully degenerate quasi-energy spectrum. To harness the flat-band protocol for stabilizing the DTC phase in the presence of such rotational errors, it is necessary to modify the Hamiltonian to maintain an effective spin-spin interaction term that can counteract the effects of spin-rotation imperfections (which is generic in MBL induced DTC). Accordingly, we introduce an additional aperiodic spin-spin interaction term to the two-tone flat-band Hamiltonian from Eq.(1a), as described below.

$$\tilde{H}_{\text{FB}}(t) = \lambda_1(t) \sum_i \hat{\sigma}_i^x \hat{\sigma}_{i+1}^x + \lambda_2(t) \sum_i \hat{\sigma}_i^z + \lambda_f J \sum_i \hat{\sigma}_i^z \hat{\sigma}_{i+1}^z, \quad (\text{B1})$$

where, the time-dependent coefficients are redefined as:

$$\begin{aligned} \lambda_1(t) &= +\lambda_0 & ; \frac{mT}{4} < t \leq \frac{(m+1)T}{4}, \\ &= -\lambda_0 & ; \frac{(m+1)T}{4} < t \leq \frac{(m+2)T}{4}, \\ \lambda_2(t) &= \omega_0 - \omega_1 & ; \frac{qT}{4p} < t \leq \frac{(q+1)T}{4p}, \\ &= \omega_0 + \omega_1 & ; \frac{(q+1)T}{4p} < t \leq \frac{(q+2)T}{4p}, \end{aligned} \quad (\text{B2})$$

Here, λ_f represents a dc-offset to the spin-spin interaction strength, and for analytical convenience, the time coefficients are fixed at $m, q = 0, 2, 4, \dots$. Here 'p' can be any integer, for simplicity, we set it to $p = 2$. Additionally, we consider $\omega_0 = 0$. The time evolution operator $\hat{U}(T, 0)$ for this modified Hamiltonian can be expressed as:

$$\hat{U}(T, 0) = \mathcal{T} (\hat{U}_4 \hat{U}_3 \hat{U}_2 \hat{U}_1 \hat{U}_0), \quad (\text{B3})$$

where the unitary operators \hat{U}_i for $i = 0, 1, 2, 3, 4$ are defined as:

$$\hat{U}_0 = \exp\left(-i\hat{H}_0\frac{T}{2}\right), \quad \hat{H}_0 = \lambda_s(1 - \varepsilon_r) \sum_i \hat{\sigma}_i^x, \quad (\text{B4})$$

$$\hat{U}_1 = \exp\left(-i\hat{H}_1\frac{T}{8}\right), \quad \hat{H}_1 = \lambda_f\hat{A} - \lambda_0\hat{B} + \omega_1\hat{C}, \quad (\text{B5})$$

$$\hat{U}_2 = \exp\left(-i\hat{H}_2\frac{T}{8}\right), \quad \hat{H}_2 = \lambda_f\hat{A} - \lambda_0\hat{B} - \omega_1\hat{C}, \quad (\text{B6})$$

$$\hat{U}_3 = \exp\left(-i\hat{H}_3\frac{T}{8}\right), \quad \hat{H}_3 = \lambda_f\hat{A} + \lambda_0\hat{B} + \omega_1\hat{C}, \quad (\text{B7})$$

$$\hat{U}_4 = \exp\left(-i\hat{H}_4\frac{T}{8}\right), \quad \hat{H}_4 = \lambda_f\hat{A} + \lambda_0\hat{B} - \omega_1\hat{C}, \quad (\text{B8})$$

and $\hat{A} = \sum_i J\hat{\sigma}_i^z\hat{\sigma}_{i+1}^z$, $\hat{B} = J \sum_i \hat{\sigma}_i^x\hat{\sigma}_{i+1}^x$, $\hat{C} = \sum_i \hat{\sigma}_i^z$. We apply the Magnus expansion [81] to approximate the time evolution operator as:

$$\begin{aligned} \hat{U}(T, 0) &= \mathcal{T} \exp\left(\int_0^T dt \hat{H}(t)\right) \\ &= \exp(-i\hat{H}_{\text{ME}}T), \end{aligned}$$

where \hat{H}_{ME} is the effective Hamiltonian derived from the Magnus expansion, which provides this as a series;

$$\hat{H}_{\text{ME}} = \sum_{n=0}^{\infty} T^n \xi_n. \quad (\text{B9})$$

$$\hat{H}_{\text{ME}} = \frac{\lambda_f J}{2} \sum_i \hat{\sigma}_i^z \hat{\sigma}_{i+1}^z + \frac{\lambda_s(1 - \varepsilon_r)}{2} \sum_i \hat{\sigma}_i^x - \frac{\lambda_s \lambda_f J T}{4} \sum_i \left(\hat{\sigma}_i^y \hat{\sigma}_{i+1}^z + \hat{\sigma}_i^z \hat{\sigma}_{i+1}^y \right) + \dots \quad (\text{B14})$$

We can express the effective Hamiltonian in generic form as follows.

$$\hat{H}_{\text{ME}} \equiv \frac{\lambda_f J}{2} \sum_i \hat{\sigma}_i^z \hat{\sigma}_{i+1}^z + \frac{\lambda_s(1 - \varepsilon_r)}{2} \sum_i \hat{\sigma}_i^x + \hat{O}(T). \quad (\text{B15})$$

Here, $\hat{O}(T)$ denote the leading-order correction arising from the non-commuting nature of the drive components. In Eq. (B15), the first term encodes the additional spin-spin interaction, while the second term realizes the spin-flip operation; since $\lambda_s T = \pi$, the latter is frequency independent. Unitary evolution is governed by $\hat{U}(T, 0) = \exp(-i\hat{H}_{\text{ME}}T)$, where the effective spin interaction strength is characterized by $\eta \equiv \frac{\lambda_f J}{\omega}$. The mitigation effect of spin-rotation errors requires η to be large enough to compensate for the melting of the DTC order for finite ε_r . Furthermore, for typical parameter regimes where $\lambda_f J, \omega_0 \ll \lambda_0, \omega_1$, the correction term $\hat{O}(T)$ remains negligible.

In the high-frequency regime, the correction term is strongly suppressed, and the stability of the DTC under finite ε_r is

Taking into account the fastest drive frequency $\Omega = 2\omega$, we divide the total time period T into five intervals, consisting of one $T/2$ for the spin flip operation and four of equal duration $T/8$. The Hamiltonians in each interval are denoted as H_i for $i = 0, 1, 2, 3, 4$. The Magnus expansion terms can be computed using these Hamiltonians.

The first-order term of the Magnus expansion is given by:

$$\begin{aligned} \xi_0 &= \frac{1}{T} \int_0^T \hat{H}(t_1) dt_1 \equiv \sum_{k=0}^{2p-1} \hat{H}_k \\ &= \frac{1}{T} \left\{ \hat{H}_0 \frac{T}{2} + (\hat{H}_1 + \hat{H}_2 + \hat{H}_3 + \hat{H}_4) \frac{T}{8} \right\}. \end{aligned} \quad (\text{B10})$$

Calculating this, we find the following.

$$\xi_0 = \frac{1}{2} \left(\lambda_s(1 - \varepsilon_r) \sum_i \hat{\sigma}_i^x + \lambda_f J \sum_i \hat{\sigma}_i^z \hat{\sigma}_{i+1}^z \right). \quad (\text{B11})$$

The second-order term is given by:

$$\xi_1 = \frac{i}{2T} \sum_{i>j} [\hat{H}_i, \hat{H}_j]. \quad (\text{B12})$$

Evaluating this term, we obtain the following.

$$\xi_1 = -\frac{\lambda_s \lambda_f J T^2}{4} \sum_i \left(\hat{\sigma}_i^y \hat{\sigma}_{i+1}^z + \hat{\sigma}_i^z \hat{\sigma}_{i+1}^y \right). \quad (\text{B13})$$

For small offsets and transverse field oscillation amplitudes, we may assume that $\lambda_f J < \omega_1 < \lambda_0$. Thus,

governed by the competition between the interaction and spin-flip terms. When interactions are weak, η is negligible, and the imperfect spin-flip term dominates, inducing beating in the temporal order parameter and ultimately destabilizing the DTC phase. In contrast, strong interactions ($\eta \gg 1$) effectively counteract rotational imperfections and preserve the phase.

Reducing the frequency causes the correction term $\hat{O}(T)$ to become appreciable. For strong interactions, its non-trivial interplay with the spin-flip and interaction terms generates complex dynamics that undermine DTC stability. In the weak-interaction regime, however, the correction remains negligible due to small interaction terms. Importantly, at low frequencies, even weak interactions produce $\eta \gg 1$ at the small denominator ω , allowing the interaction term to compensate for spin-rotation errors and maintain a robust subharmonic response.

Nevertheless, a more comprehensive investigation is needed to determine how the additional interaction term and the correction term jointly govern DTC stability across the full parameter space, despite the perfectly unitary dynamics of the

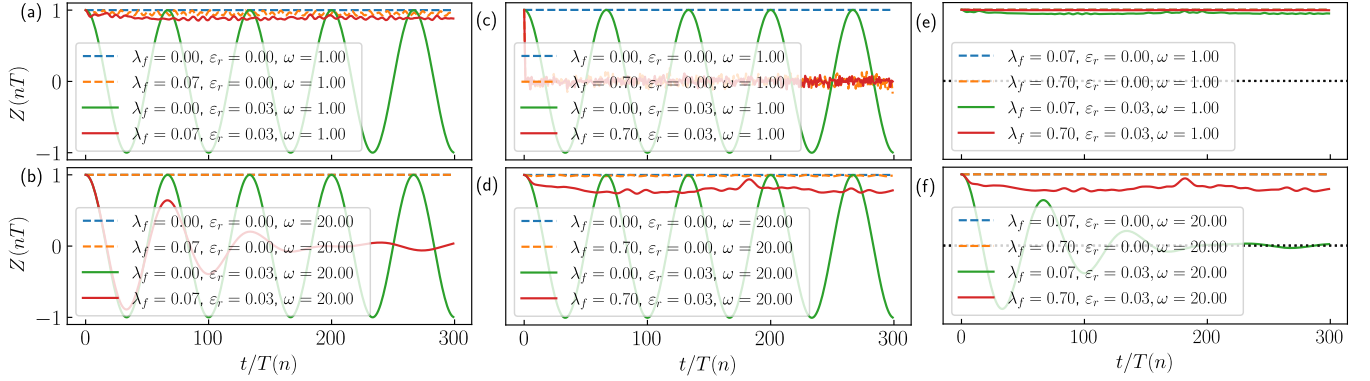


FIG. 12. Comparative stability analysis of the DTC phase under the modified flat-band protocol. Panels (a–d) present results incorporating flat-band and an additional dc interaction term ($\lambda_f J$), while panels (e,f) show results only due to the interaction term ($\lambda_f J$). The analysis spans two interaction regimes—strong interactions [$\lambda_0 = 1$, panels (a,b)] and weak interactions [$\lambda_0 = 0.1$, panels (c,d)]—across both high-frequency ($\omega = 20$) and low-frequency ($\omega = 1$) driving regimes. Compared to Fig. 11, the modified protocol demonstrates qualitatively distinct DTC behavior in presence of additional interactions (panels: a-d) and absence of flat-band (panels: e,f), corroborating the emergent stable DTC phase in presence of mutual interaction between flat-band and additional interaction term. All simulations were performed for a spin chain of size $N = 8$, with parameters fixed at $\lambda_f = 0.7\lambda_0$, $J = 1$ and $\omega_0 = 0.0$.

exact flat-band protocol. Our results show that the added terms λ_f stabilize the DTC phase only in regimes where the correction term in Eq. B15 is negligible; once this term becomes appreciable, the robustness of the phase deteriorates. Hence, DTC stability is controlled not by the absolute magnitude of the further added interactions alone, but by their nontrivial interplay with the correction term (see Fig. 12), which can

either strengthen or weaken localization and the associated subharmonic response depending on the parameter regime.

Taken together, these findings indicate that the flat-band protocol, combined with an additional spin-spin interaction, provides a viable route to stabilizing the DTC phase against spin-rotation errors in two distinct regimes: high-frequency driving with strong interactions and low-frequency driving with weak interactions.

-
- [1] B. M. Walter Greiner, *Quantum Mechanics* (Springer Berlin Heidelberg, 2012).
- [2] F. Strocchi, *Symmetry Breaking* (Springer Berlin Heidelberg, 2021).
- [3] C. M. Bender and D. W. Hook, *Rev. Mod. Phys.* **96**, 045002 (2024).
- [4] H. Ziaepour, *Journal of Physics: Conference Series* **626**, 012074 (2015).
- [5] O. Lombardi and S. Fortin, The role of symmetry in the interpretation of quantum mechanics (2016), arXiv:1602.07160.
- [6] G. Mack and V. Schomerus, *Journal of Geometry and Physics* **11**, 361 (1993).
- [7] D. Harlow and H. Ooguri, *Communications in Mathematical Physics* **383**, 1669 (2021).
- [8] C. M. Bender, A. Felski, S. P. Klevansky, and S. Sarkar, *Journal of Physics: Conference Series* **2038**, 012004 (2021).
- [9] B. Gripaos, O. Randal-Williams, and J. Tooby-Smith, *Journal of Geometry and Physics* **201**, 105212 (2024).
- [10] S. WILLENBROCK, *Symmetries of the standard model, in Physics In D >= 4 Tasi 2004* (World Scientific, 2004) pp. 3–38.
- [11] J. Bernabeu, *Symmetries in the standard model, in Fundamental Physics and Physics Education Research*, edited by B. G. Sidharth, J. C. Murillo, M. Michelini, and C. Perea (Springer International Publishing, Cham, 2021) pp. 3–16.
- [12] R. Matthew, *Mathematics and particle physics, in Symmetry and the Standard Model* (Springer New York, NY, 2014) pp. XIX, 327.
- [13] C. Wu, The symmetry principle in condensed matter physics (i), in *A Festschrift in Honor of the C N Yang Centenary* (WORLD SCIENTIFIC, 2022) p. 413–473.
- [14] J. McGreevy, *Annual Review of Condensed Matter Physics* **14**, 57 (2023).
- [15] N. S. Yanofsky and M. Zelcer, *Foundations of Science* **22**, 495 (2017).
- [16] T. Brauner, *Spontaneous symmetry breaking, in Effective Field Theory for Spontaneously Broken Symmetry* (Springer International Publishing, Cham, 2024) pp. 61–84.
- [17] L. D. Landau and E. M. Lifshitz, *Statistical Physics*, 3rd ed. (Butterworth-Heinemann, Oxford, England, 1996).
- [18] N. Goldenfeld, *Lectures on Phase Transitions and the Renormalization Group* (Addison-Wesley, 1992).
- [19] D. J. Thouless, M. Kohmoto, M. P. Nightingale, and M. den Nijs, *Phys. Rev. Lett.* **49**, 405 (1982).
- [20] M. O. Goerbig, *Quantum hall effects* (2009), arXiv:0909.1998 [cond-mat.mes-hall].
- [21] D. Basko, I. Aleiner, and B. Altshuler, *Annals of Physics* **321**, 1126 (2006).
- [22] R. Nandkishore and D. A. Huse, *Annual Review of Condensed Matter Physics* **6**, 15–38 (2015).
- [23] V. Khemani, S. P. Lim, D. N. Sheng, and D. A. Huse, *Phys. Rev. X* **7**, 021013 (2017).
- [24] D. A. Abanin, E. Altman, I. Bloch, and M. Serbyn, *Reviews of*

- Modern Physics **91**, 10.1103/revmodphys.91.021001 (2019).
- [25] F. Iemini, A. Russomanno, J. Keeling, M. Schirò, M. Dalmonte, and R. Fazio, *Phys. Rev. Lett.* **121**, 035301 (2018).
- [26] B. Buča, J. Tindall, and D. Jaksch, *Nature Communications* **10**, 10.1038/s41467-019-09757-y (2019).
- [27] K. Sacha, *Time Crystals*, Springer Series on Atomic, Optical, and Plasma Physics, Vol. 114 (Springer International Publishing, 2021).
- [28] A. Shapere and F. Wilczek, *Physical Review Letters* **109**, 10.1103/physrevlett.109.160402 (2012).
- [29] F. Wilczek, *Phys. Rev. Lett.* **109**, 160401 (2012).
- [30] P. Bruno, *Phys. Rev. Lett.* **111**, 070402 (2013).
- [31] P. Nozières, *Europhysics Letters* **103**, 57008 (2013).
- [32] H. Watanabe and M. Oshikawa, *Phys. Rev. Lett.* **114**, 251603 (2015).
- [33] K. Sacha, *Phys. Rev. A* **91**, 033617 (2015).
- [34] D. V. Else, B. Bauer, and C. Nayak, *Phys. Rev. Lett.* **117**, 090402 (2016).
- [35] J. Zhang, P. W. Hess, A. Kyprianidis, P. Becker, A. Lee, J. Smith, G. Pagano, I.-D. Potirniche, A. C. Potter, A. Vishwanath, N. Y. Yao, and C. Monroe, *Nature* **543**, 217 (2017).
- [36] M. Ippoliti, K. Kechedzhi, R. Moessner, S. Sondhi, and V. Khemani, *PRX Quantum* **2**, 030346 (2021).
- [37] J.-y. Choi, *Journal of the Korean Physical Society* **82**, 875 (2023).
- [38] A. Russomanno, F. Iemini, M. Dalmonte, and R. Fazio, *Phys. Rev. B* **95**, 214307 (2017).
- [39] J. M. Deutsch, *Phys. Rev. A* **43**, 2046 (1991).
- [40] M. Srednicki, *Phys. Rev. E* **50**, 888 (1994).
- [41] J. Hauschild, F. Heidrich-Meisner, and F. Pollmann, *Phys. Rev. B* **94**, 161109 (2016).
- [42] R. Chandra, M. Rahaman, S. Majumder, A. Roy, and S. Sarkar, *Integrable floquet time crystals in one dimension* (2025), arXiv:2510.04326 [cond-mat.str-el].
- [43] R. Schäfer, G. S. Uhrig, and J. Stolze, *Physical Review B* **100**, 184301 (2019).
- [44] M. Rahaman, A. Sakurai, and A. Roy, *New Journal of Physics* **26**, 063035 (2024).
- [45] W. C. Yu, J. Tangpanitanon, A. W. Glaetzle, D. Jaksch, and D. G. Angelakis, *Phys. Rev. A* **99**, 033618 (2019).
- [46] B. Huang, Y.-H. Wu, and W. V. Liu, *Phys. Rev. Lett.* **120**, 110603 (2018).
- [47] S. Anisur, W. V. Liu, and S. Choudhury, *Entropy* **27**, 10.3390/e27060609 (2025).
- [48] S. Choudhury, *Atoms* **9**, 10.3390/atoms9020025 (2021).
- [49] C. Lyu, S. Choudhury, C. Lv, Y. Yan, and Q. Zhou, *Phys. Rev. Res.* **2**, 033070 (2020).
- [50] H. Biswas and S. Choudhury, *Discrete time crystals in the spin-s central spin model* (2025), arXiv:2505.13207 [quant-ph].
- [51] H. Biswas and S. Choudhury, *The floquet central spin model: A platform to realize eternal time crystals, entanglement steering, and multiparameter metrology* (2025), arXiv:2501.18472 [quant-ph].
- [52] L. Zhang, V. Khemani, and D. A. Huse, *Phys. Rev. B* **94**, 224202 (2016).
- [53] N. Y. Yao, A. C. Potter, I.-D. Potirniche, and A. Vishwanath, *Phys. Rev. Lett.* **118**, 030401 (2017).
- [54] J. Randall, C. E. Bradley, F. V. van der Gronden, A. Galicia, M. H. Abobeih, M. Markham, D. J. Twitchen, F. Machado, N. Y. Yao, and T. H. Taminiou, *Science* **374**, 1474 (2021).
- [55] S. Choi, J. Choi, R. Landig, G. Kucsko, H. Zhou, J. Isoya, F. Jelezko, S. Onoda, H. Sumiya, V. Khemani, C. von Keyserlingk, N. Y. Yao, E. Demler, and M. D. Lukin, *Nature* **543**, 221 (2017).
- [56] A. Pizzi, J. Knolle, and A. Nunnenkamp, *Nature Communications* **12**, 2341 (2021).
- [57] V. K. Kozin and O. Kyriienko, *Physical Review Letters* **123**, 210602 (2019).
- [58] A. Das, *Phys. Rev. B* **82**, 172402 (2010).
- [59] A. Haldar, D. Sen, R. Moessner, and A. Das, *Phys. Rev. X* **11**, 021008 (2021).
- [60] M. Rahaman, T. Mori, and A. Roy, *Phys. Rev. B* **109**, 104311 (2024).
- [61] S. Ashhab, J. R. Johansson, A. M. Zagoskin, and F. Nori, *Phys. Rev. A* **75**, 063414 (2007).
- [62] A. Morningstar, L. Colmenarez, V. Khemani, D. J. Luitz, and D. A. Huse, *Phys. Rev. B* **105**, 174205 (2022).
- [63] T. Banerjee, S. Choudhury, and K. Sengupta, *New Journal of Physics* **27**, 084506 (2025).
- [64] K. Ghosh, S. Choudhury, D. Sen, and K. Sengupta, *Phys. Rev. B* **112**, 155142 (2025).
- [65] U. Divakaran and K. Sengupta, *Phys. Rev. B* **90**, 184303 (2014).
- [66] J. Naji, R. Jafari, L. Zhou, and A. Langari, *Phys. Rev. B* **106**, 094314 (2022).
- [67] J. D. Sau and K. Sengupta, *Phys. Rev. B* **90**, 104306 (2014).
- [68] N. Lambert, E. Giguère, P. Menczel, B. Li, P. Hopf, G. Suárez, M. Gali, J. Lishman, R. Gadhvi, R. Agarwal, A. Galicia, N. Shammah, P. Nation, J. R. Johansson, S. Ahmed, S. Cross, A. Pitchford, and F. Nori, *Qutip 5: The quantum toolbox in python* (2024), arXiv:2412.04705 [quant-ph].
- [69] J. H. Shirley, *Phys. Rev.* **138**, B979 (1965).
- [70] H. Sambe, *Phys. Rev. A* **7**, 2203 (1973).
- [71] M. Holthaus, *Journal of Physics B: Atomic, Molecular and Optical Physics* **49**, 013001 (2015).
- [72] G. B. Mbeng, A. Russomanno, and G. E. Santoro, *SciPost Physics Lecture Notes*, 082 (2024).
- [73] A. S. Buyskikh, M. Fagotti, J. Schachenmayer, F. Essler, and A. J. Daley, *Phys. Rev. A* **93**, 053620 (2016).
- [74] V. Khemani, A. Lazarides, R. Moessner, and S. L. Sondhi, *Phys. Rev. Lett.* **116**, 250401 (2016).
- [75] J. Preskill, *Quantum* **2**, 79 (2018).
- [76] A. Browaeys and T. Lahaye, *Nature Physics* **16**, 132 (2020).
- [77] N. Hatano and M. Suzuki, *Finding exponential product formulas of higher orders*, in *Quantum Annealing and Other Optimization Methods*, edited by A. Das and B. K. Chakrabarti (Springer Berlin Heidelberg, Berlin, Heidelberg, 2005) pp. 37–68.
- [78] F. Casas, A. Murua, and M. Nadinic, *Computer Physics Communications* **183**, 2386 (2012).
- [79] L. Dupays and J.-C. Pain, *Journal of Physics A: Mathematical and Theoretical* **56**, 255202 (2023).
- [80] T. Kimura, *Progress of Theoretical and Experimental Physics* **2017**, 041A03 (2017).
- [81] T. Kuwahara, T. Mori, and K. Saito, *Annals of Physics* **367**, 96 (2016).